CHEMISTRY
AN ASIAN JOURNAL

DOI: 10.1002/asia.200600137

Design of Dual-Emission Chemosensors for Ratiometric Detection of ATP Derivatives

Akio Ojida,[a] Yoshifumi Miyahara,[a] Jirarut Wongkongkatep,[a] Shun-ichi Tamaru,[a] Kazuki Sada,[b] and Itaru Hamachi*[a]

Abstract: Nucleoside pyrophosphate (nucleoside PP) derivatives are widespread in living cells and play pivotal roles in various biological events. We report novel fluorescence chemosensors for nucleoside PPs that make use of coordination chemistry. The chemosensors, which contain two Zn^{II}–dipicolylamine units, bind strongly to nucleoside PPs ($K_{app} > 10^6\,M^{-1}$) in aqueous solution and sense them by a dual-emission change. Detailed fluorescence and UV/Vis spectral studies revealed that the emission changes of the chemosensors upon binding to nucleoside PPs can be ascribed to the loss of coordination between Zn^{II} and the acridine fluorophore. This is a unique sensing system based on the anion-induced rearrangement of the coordination. Furthermore, we demonstrated the utility of these chemosensors in real-time monitoring of two important biological processes involving nucleoside PP conversion: the apyrase-catalyzed hydrolysis of nucleoside PPs and the glycosyl transfer catalyzed by β-1,4-galactosyltransferase.

Keywords: anions · coordination chemistry · enzymes · fluorescent probes · sensors

Introduction

Nucleoside pyrophosphate (nucleoside PP) derivatives are widespread in living cells and play pivotal roles in various biological events.[1] All cells maintain a high intracellular concentration of ATP, which acts as a ubiquitous energy source for various metabolic cycles in all tissues. Furthermore, nucleoside PPs are involved in many enzymatic processes as reactive substrates. For example, ATP serves as a phosphate donor in kinase-catalyzed protein phosphorylation, and UDP glycosides are used as substrates in many glycosylation processes catalyzed by glycosyltransferases. Besides these fundamental intracellular roles, nucleoside PPs such as ATP, ADP, and a variety of diadenosine polyphosphates also play important extracelluar roles as signaling substances.[2] In particular, extracellular ATP released from the cell membrane mediates many cell-to-cell signals in a large variety of physiological and pathological conditions. Therefore, considerable effort has been devoted to the development of rapid and convenient determination systems for nucleoside PP derivatives. These include a luciferin–luciferase bioluminescence assay, an electrochemical sensor coupled with sequential enzyme reactions, biosensors that use the patch–clamp technique, and so on.[3] Alternatively, fluorescence detection with a small molecule-based chemosensor has great promise for biological assays, including those for the production or metabolism of nucleoside PPs. This is a straightforward technique with high sensitivity and rapid response, which promises real-time detection of nucleoside PPs under various biological conditions without special skills or instruments. Owing to the overall benefits of fluorescence detection, there has been great interest in developing a selective fluorescent chemosensor for PP derivatives.[4] However, despite the many artificial receptors or chemosensors for phosphate species developed for molecular recognition, a limited number work efficiently in aqueous conditions, and few bioanalytical applications have been reported so far.[5,6]

In fluorescence detection, ratiometric sensing has several advantages, including enhanced dynamic range, precise cor-

[a] Dr. A. Ojida, Y. Miyahara, Dr. J. Wongkongkatep, Dr. S.-i. Tamaru, Prof. I. Hamachi
Department of Synthetic Chemistry and Biological Chemistry
Graduate School of Engineering, Kyoto University
Katsura Campus, Nishikyo-ku, Kyoto, 615-8510 (Japan)
Fax: (+81) 75-383-2759
E-mail: ihamachi@sbchem.kyoto-u.ac.jp

[b] Dr. K. Sada
Department of Chemistry and Biochemistry
Graduate School of Engineering, Kyushu University
Fukuoka, 819-0395 (Japan)

Supporting information for this article is available on the WWW under http://www.chemasianj.org or from the author.

rection without interference by environmental effects, and convenient visual monitoring; thus, it is suitable for bioanalytical measurements. A number of fluorescent ratiometric sensors for cations such as Na^+, K^+, Ca^{2+}, Zn^{2+}, Mg^{2+}, and so on have been developed, some of which were applied to biological studies.[7] A successful example is intracellular Ca^{2+} imaging with fluorescent chemosensors such as fura, indo, and calcium green. These chemosensors enable precise determination of cytosolic free Ca^{2+} concentration inside living cells owing to changes in dual emission or excitation upon binding to Ca^{2+} and, consequently, have contributed greatly to the understanding of the dynamics of Ca^{2+} ions in various cell-signaling pathways. In contrast to such successful developments of ratiometric cation sensors, dual-emission sensors capable of ratiometric analysis for anions have hardly been developed so far.[6b,8] This is partly due to the general difficulty of development of anion sensors that operate in aqueous medium and, more seriously, the lack of sensing mechanisms available to detect the anion binding event by the shift in the fluorescence emission/excitation wavelength. Herein we describe new dual-emission chemosensors for nucleoside PPs that operate under neutral aqueous conditions. These chemosensors can bind strongly to nucleoside PPs such as ATP and ADP ($K_{app} > 10^6\,M^{-1}$) by making use of coordination chemistry and detect them by changes in dual emission, thus allowing ratiometric nucleoside PP analysis. The mechanism of the dual-emission sensing involves a change in the coordination between the acridine fluorophore and the Zn^{II} ions upon binding to a nucleoside PP, which is experimentally supported by X-ray crystal analysis and detailed spectroscopic studies. Based on the ratiometric sensing mode, these chemosensors were successfully applied to the real-time fluorescence assay of two important biological processes: the apyrase-catalyzed hydrolysis of nucleoside PPs and glycosyl transfer catalyzed by β-1,4-galactosyltransferase.

Abstract in Japanese:

ヌクレオシドリン酸種は様々な生体内機能において重要な役割を果たすアニオン種である。この論文ではヌクレオシドリン酸種を二波長レシオ型の蛍光変化で検出する新しい亜鉛錯体型ケモセンサーについて報告する。このケモセンサーはアクリジンを蛍光団として有しており、二つのジピコリルアミン一亜鉛錯体部位でヌクレオシドリン酸種と強く結合する。蛍光や UV/Vis 吸収スペクトルによる詳しい分光学的解析から、ヌクレオシドリン酸種と相互作用した際のケモセンサーの蛍光波長変化メカニズムは、アクリジン蛍光団と亜鉛イオンとの配位相互作用の解消であることが明らかとなった。このケモセンサーの有用性は、酵素アピレースによるヌクレオシドリン酸種の加水分解反応、および糖転移酵素によるグリコシル結合形成反応のリアルタイム蛍光モニタリングにおいて有意に示された。

Results and Discussion

Molecular Design, Synthesis, and Structure of the Chemosensors

To carry out ratiometric analysis, two distinct changes in fluorescence emission or excitation are required within a single molecular system. Most ratiometric cation sensors reported to date are designed to conjugate a cation binding site with a fluorophore in a direct manner so that the cation binding event influences the photochemical properties of the fluorophore to express a dual-emission change.[7] We planned to utilize such a metal-cation-induced change in fluorescence emission/excitation for ratiometric anion sensing (Figure 1). According to the literature,[9] acridine fluorophore shows a bathochromic emission shift on protonation or metal-cation coordination to its central nitrogen atom. Thus it may be a candidate for two distinct emissions depending on its electronic configuration. On the basis of our previous work on the anthracene-type Zn^{II} complex **4**–2Zn^{II} as a fluorescent chemosensor for biological phosphate species,[10] we designed new chemosensors **1**–2Zn^{II} and **2**–2Zn^{II} that contain an acridine moiety as a fluorophore (Figure 2). It is anticipated that the anion binding on the Zn^{II}–Dpa sites disturbs the interaction between Zn^{II} and the acridine fluorophore by coordination exchange, which restores the electronic property of the acridine to its original noncoordinated

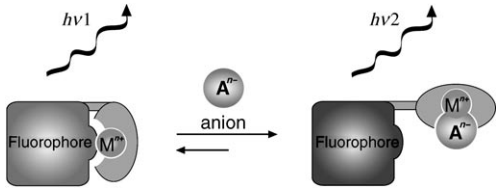

Figure 1. The dual-emission anion-sensing system reported herein.

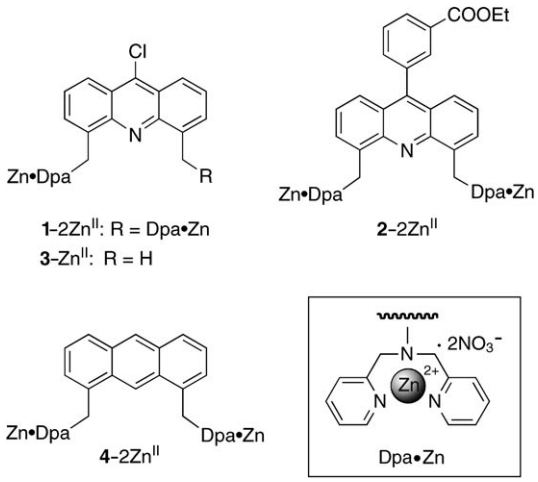

Figure 2. The chemical structure of the chemosensors. Dpa = 2,2′-dipicolylamine.

state, thus resulting in a shift in the emission/excitation wavelength (Figure 1).

The synthesis of **1**–2Zn^{II} and **2**–2Zn^{II} was carried out as described in Scheme 1. Both chemosensors were prepared from 9-chloroacridine (**6a**), which was obtained by the intramolecular cyclization of *N*-aryl anthranylic acid (**5a**).[11] The radical bromination of **6a** and the subsequent nucleophilic substitution with Dpa gave ligand **1**. Ligand **2** was synthesized by Suzuki coupling to introduce an aryl substituent at the 9-position of **6a** followed by bromination and Dpa substitution. Ligands **1** and **2** were treated with zinc(II) nitrate (2 equiv) in aqueous MeOH to give the chemosensors **1**–2Zn^{II} and **2**–2Zn^{II}. By using the same synthetic procedures, chemosensor **3**–Zn^{II} was prepared as a monodentate control compound. Characterization of these compounds was performed with ^{1}H NMR spectroscopy, mass spectrometry, and elemental analysis. Detailed synthetic procedures and compound characterizations are described in the Supporting Information. The structure of **1**–2Zn^{II} was successfully investigated by X-ray crystallographic analysis.[12] Crystallization of the binuclear **1**–2Zn^{II} from MeOH yielded a single crystal suitable for structural analysis. The structure of **1**–2Zn^{II} is displayed in Figure 3. Both Zn^{II} ions have a disordered trigonal-bipyramidal coordination geometry, each of which is coordinated by the three nitrogen atoms of Dpa and two nitrate anions. Coordination of Zn^{II} to the acridine nitrogen atom was not observed in this binuclear Zn^{II} complex. However, this coordination bond evidently exists in the case of the mononuclear Zn^{II} complex of **1** under aqueous conditions, and plays a key role in the ratiometric fluorescence detection for the nucleoside PPs (see below).

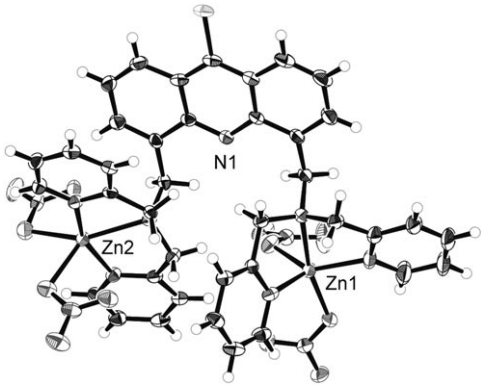

Figure 3. ORTEP drawing (50% probability ellipsoids) of binuclear Zn^{II} complex **1**–2Zn^{II}·4NO$_3$. The disordered MeOH molecules are omitted for clarity.

Anion Binding and Selectivity of Fluorescence Sensing

When **1**–2Zn^{II} and **2**–2Zn^{II} were excited at 368 nm, absorption maxima were observed at 363 nm and emission maxima at 468 nm (see Supporting Information). The fluorescence quantum yields of **1**–2Zn^{II} and **2**–2Zn^{II} were 0.04 and 0.16, respectively, in aqueous HEPES buffer (pH 7.2), determined by using quinine sulfate in H_2SO_4 (0.1 N) as the standard. Upon addition of ATP to **1**–2Zn^{II} (10 μM) under neutral aqueous conditions (50 mM HEPES, pH 7.2), the emission maximum at 468 nm immediately decreased in intensity and underwent a blue shift to 441 nm (Figure 4a), unlike the anthracene-type chemosensor **4**–2Zn^{II}, which showed simple fluorescence intensification.[10] The much clearer wavelength shift and the change in emission intensity upon ATP binding resulted in a seesaw-type spectral change in the case of **2**–2Zn^{II} (Figure 4b,c). Under these conditions, **2**–2Zn^{II} (10 μM) was able to detect 10^{-7} M of ATP with a clear dual-emission change, but not 10^{-8} M ATP (data not shown). When a higher concentration of **1**–2Zn^{II} (30 μM) was used, the fluorescence change halted sharply at 1 equivalent of ATP, thus indicating that the binding stoichiometry between the chemosensors and ATP is 1:1 (see Supporting Information). On the other hand, the monodentate Zn^{II}–Dpa complex **3**–Zn^{II} did not show any fluorescence change on addition of ATP (data not shown). This indicates that the two Zn^{II}–Dpa sites of **1**–2Zn^{II} and **2**–2Zn^{II} interact simultaneously with the PP site of ATP through metal–ligand interactions that show a strong affinity in aqueous solution. In ^{31}P NMR spectroscopic experiments (0.5 mM, HEPES (50 mM, pH 7.2) containing D_2O (10%)), **1**–2Zn^{II} induced downfield shifts of the peaks corresponding to β and γ phosphate units of ATP from −19.4 and −5.5 ppm to −16.9 and −2.4 ppm, respectively, whereas the peak of the α phosphate

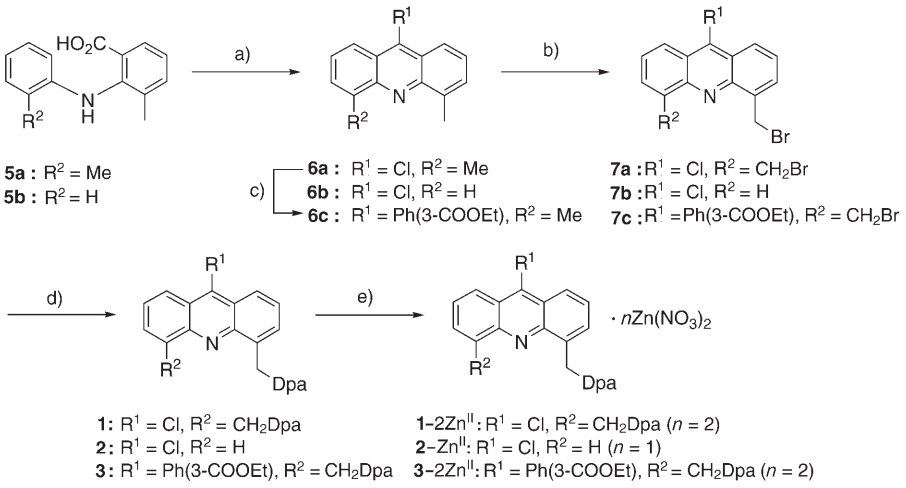

Scheme 1. Preparation of the chemosensors. a) $POCl_3$, reflux; b) *N*-bromosuccinimide, benzoyl peroxide, CCl_4, reflux; c) ethyl 3-(4,4,5,5-tetramethyl-1,3,2-dioxaborolan-2-yl)benzoate, [Pd_2(dibenzylideneacetone)$_3$], 2-(di-*tert*-butylphosphanyl)biphenyl, Cs_2CO_3, *N*,*N*-dimethylformamide (DMF), 80 °C; d) Dpa, K_2CO_3, DMF, room temperature; e) $Zn(NO_3)_2$, MeOH/H_2O, room temperature.

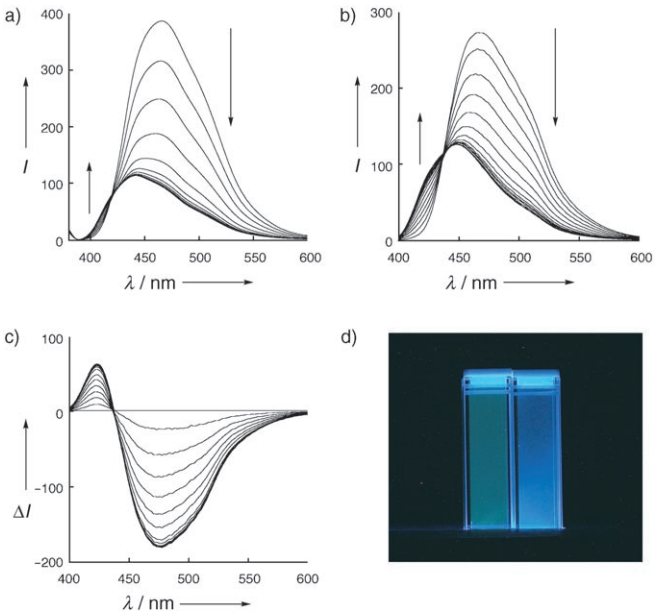

Figure 4. Changes in the fluorescence emission of the chemosensors induced by nucleoside PP. a) Changes in the emission spectrum of **1**–2Zn^{II} (10 μM) upon addition of ATP. [ATP] = 0, 2, 4, 6, 8, 10, 12, 14, 16, 18, 20 μM. b) Changes in the emission spectrum and c) changes in the difference spectrum of **2**–2Zn^{II} (10 μM) upon addition of ATP. [ATP] = 0, 2, 4, 6, 8, 10, 12, 14, 16, 18, 20, 24, 32, 40 μM. ΔI = difference in fluorescence intensity from the initial state ([ATP] = 0 μM). Conditions: HEPES buffer (50 mM), NaCl (10 mM), pH 7.2, 20 °C, λ_{ex} = 368 nm. d) Photograph of the fluorescence emission of **2**–2Zn^{II} in the absence (left) and presence (right) of ATP. The arrows in a) and b) show the direction of change of the spectrum at that position as ATP concentration is increased.

Table 1. Apparent binding constants (K_{app}) of **1**–2Zn^{II} and **2**–2Zn^{II} to various anions determined by changes in fluorescence.

Anion species[a]	K_{app} [M^{-1}][b]		Anion species[a]	K_{app} [M^{-1}][b]	
	1–2Zn^{II}	**2**–2Zn^{II}		**1**–2Zn^{II}	**2**–2Zn^{II}
ATP	7.6×10^6	5.3×10^6	cAMP	$<10^3$	$<10^3$
ADP	1.7×10^6	2.7×10^6	cGMP	$<10^3$	$<10^3$
AMP	2.0×10^4	1.7×10^4	HPO_4^{2-}	1.1×10^4	3.6×10^4
GTP	1.7×10^7	2.2×10^7	$P_2O_7^{4-}$	–[c]	–[c]
GDP	2.4×10^6	4.2×10^6	AcO^-	–[d]	–[d]
GMP	3.3×10^4	3.4×10^4	SO_4^{2-}	–[d]	–[d]
UDP	1.3×10^6	1.7×10^6	NO_3^-	–[d]	–[d]
UDP-Gal	$<10^3$	$<10^3$	HCO_3^-	$<10^3$	$<10^3$
			Cl^-	–[d]	–[d]

[a] All counterions of the phosphate species are sodium. ATP = adenosine-5′-triphosphate, ADP = adenosine-5′-diphosphate, AMP = adenosine-5′-monophosphate, GTP = guanosine-5′-triphosphate, GDP = guanosine-5′-diphosphate, GMP = guanosine-5′-monophosphate, UDP = uridine-5′-diphosphate, UDP-Gal = uridine-5′-diphosphogalactose, cAMP = adenosine-3′,5′-cyclic monophosphate, cGMP = guanosine-3′,5′-cyclic monophosphate. [b] K_{app} values were determined by curve-fitting of the fluorescence titration data. Conditions: HEPES (50 mM), NaCl (50 mM), pH 7.2, 20 °C. [c] As the binding stoichimetry is not 1:1, the binding constant was not determined. [d] As the fluorescence changes were hardly observed, the binding constant could not be obtained.

observed at −8.03 ppm scarcely changed (data not shown). This result may suggest that both Zn^{II}–Dpa sites of **1**–2Zn^{II} predominantly interact with the β and γ phosphate groups of ATP in a chelation-like manner. Figure 4d shows a photograph of **2**–2Zn^{II} in the presence and absence of ATP. The original green fluorescence emission of **2**–2Zn^{II} turned blue in the presence of ATP. Thus, one can simply detect the nucleoside PPs by the change in emission color, which is one of the benefits of dual-emission sensing.

Subsequently, we examined the fluorescence-sensing ability of the chemosensors toward various phosphate species of biological importance. The binding constants are summarized in Table 1. Both **1**–2Zn^{II} and **2**–2Zn^{II} displayed changes in ratiometric emission upon binding to nucleoside PPs with strong binding affinities ($K_{app} > 10^6$ M^{-1}), such as ATP, GTP, ADP, GDP, and UDP. In the case of pyrophosphate anion ($P_2O_7^{2-}$), a similar dual-emission change was observed in both chemosensors. However, the change stopped at the addition of about 0.6 equivalents of pyrophosphate. This indicates that the interaction with pyrophosphate anion does not have 1:1 stoichiometry, but contains different binding modes (1:2 or higher order). Binding was relatively weak for the monophosphate derivatives such as AMP, UDP-Gal, and $H_2PO_4^{2-}$, and cAMP and cGMP did not cause any fluorescence change, which suggests that a phosphomonoester moiety involved in a pyrophosphate group is required for strong binding. Addition of millimolar concentrations of other anions (acetate, sulfate, nitrate, carbonate, and chloride) to both chemosensors did not induce significant fluorescence changes. These results indicate that **1**–2Zn^{II} and **2**–2Zn^{II} are selective fluorescent chemosensors with a ratiometric sensing mode for nucleoside PP derivatives.

Mechanism of Dual-Emission Change by Nucleoside PP Binding

The mechanism of the observed emission shift upon binding to nucleoside PPs was explored by the following experiments. In the Zn^{II} titration experiment of bis-Dpa acridine ligand **1** (20 μM in HEPES (10 mM, pH 7.2)/MeOH = 1:1), the absorption maximum at 377 nm decreased with the appearance of a new peak at 388 nm up to the addition of 1 equivalent of Zn^{II} (Figure 5a,c, Supporting Information). Almost the same spectral change was observed when the neutral solution of **1** in aqueous methanol was acidified with HCl (pH < 1) (see Supporting Information). These changes in the absorption spectra indicate that Zn^{II} coordination or protonation occurs not only to the Dpa sites but also to the acridine nitrogen atom of **1**, thus influencing the electronic properties of the acridine fluorophore. Interestingly, the observed spectral change induced by 1 equivalent of Zn^{II} was gradually cancelled to restore the original spectrum of **1** by the addition of more than 1 equivalent of Zn^{II} (Figure 5a,c, Supporting Information). This reverse change indicates the dissociation of Zn^{II} from the acridine nitrogen atom of **1** to form the binuclear **1**–2Zn^{II} complex. The coordination rearrangement induced by the second Zn^{II} complexation is probably due to electronic repulsion between the two Zn^{II} cations and/or the steric requirement for the formation of the binuclear Zn^{II} complex. In the ^{1}H NMR spectroscopic study,

CHEMISTRY
AN ASIAN JOURNAL

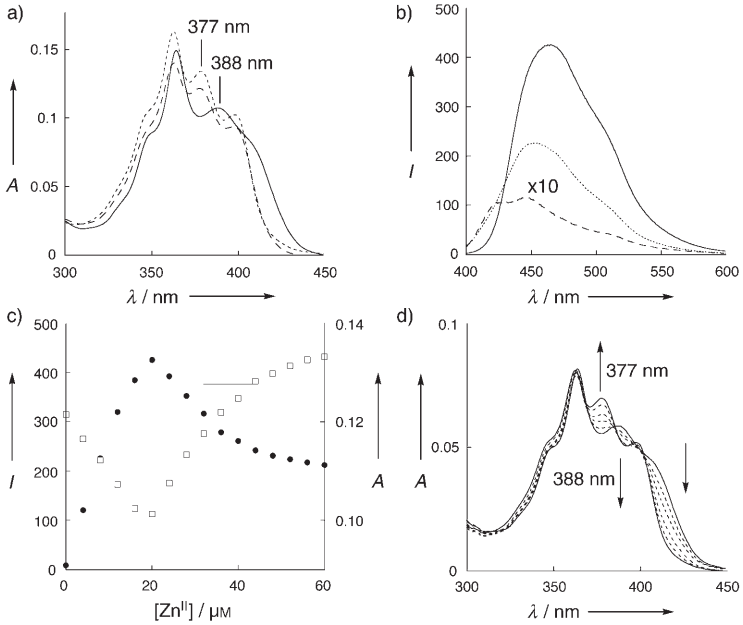

Figure 5. a) UV/Vis and b) fluorescence-emission spectra of **1** (20 μM) in the absence (– – –) and in the presence of 1 equivalent (——) or 3 equivalents (-----) of Zn^{II}. The fluorescence intensity of **1** in the absence of Zn^{II} is magnified (×10) for clarity. c) Plot of fluorescence-emission intensity (468 nm; ●) and UV absorption (377 nm; □) of **1** in the Zn^{II} titration. Conditions: HEPES buffer (10 mM, pH 7.2)/MeOH = 1/1 (*v*/*v*), 20 °C. d) Changes in the UV/Vis spectrum of **1**–2Zn^{II} (10 μM) upon addition of ATP. [ATP] = 0, 2, 4, 6, 8, 10 μM. Conditions: HEPES buffer (10 mM), pH 7.2, 20 °C. The extreme right arrow in d) indicates the direction of change of the spectrum at that position as ATP is added.

the two Dpa units of **1**–2Zn^{II} (1 mM in CD_3OD) could not be discriminated in the presence of more than 2 equivalents of Zn^{II} (data not shown), which suggests that **1**–2Zn^{II} has a highly symmetrical structure in protic solvents. This structure may be analogous to that of the binuclear complex revealed by X-ray crystallographic analysis (Figure 3).

The fluorescence emission of **1** also changed in a biphasic manner in the Zn^{II} titration experiment, together with the change in absorption. As shown in Figure 5b, the emission maximum of **1** underwent a red shift from 447 to 468 nm, with a large increase in fluorescence, upon addition of 1 equivalent of Zn^{II}, followed by a blue shift to 453 nm upon addition of more than 1 equivalent of Zn^{II} (see also the Supporting Information). The large fluorescence enhancement observed with the addition of up to 1 equivalent of Zn^{II} can be reasonably explained by inhibition of photoinduced electron transfer (PET) quenching from the tertiary amine groups of Dpa upon Zn^{II} complexation. The observed biphasic shift in fluorescence emission, which is coincident with the change in UV absorption, strongly suggests that Zn^{II} coordination with the acridine nitrogen atom induces a bathochromic emission shift similar to the case of acridine protonation reported in the literature.[9,13] In the case of the Zn^{II} titration of the mono-Dpa ligand **3**, the absorption spectrum changed in an almost-identical manner to that observed in the bis-Dpa ligand **1**, and the fluorescence emission also underwent a red shift with the addition of up to 1 equivalent of Zn^{II}, with strong fluorescence intensification as observed for **1** (see Supporting Information). However, unlike the case of **1**, the subsequent change in the absorption spectrum and emission blue shift was not induced upon addition of more than 1 equivalent of Zn^{II}. This result indicates that Zn^{II} coordinates to the acridine nitrogen atom as well as the Dpa site of **3**, and, more importantly, the subsequent spectral changes observed in the case of **1** can be ascribed to the second Zn^{II} complexation.

In aqueous HEPES buffer (pH 7.2), the observed fluorescence emission maximum ($\lambda_{em} = 463$ nm; Figure 4a) and the shape of the UV/Vis spectrum (Figure 5d) indicates that **1**–2Zn^{II} exists predominantly as a mononuclear Zn^{II} complex with coordination between the Zn^{II} ion and the acridine nitrogen atom. The complexation constant of the first and second Zn^{II} ions of **1** (K_1 and K_2 in [Eq. (1)] and [Eq. (2)]) in aqueous HEPES buffer was determined to be $>10^7$ and $1.2\times10^4\,M^{-1}$, respectively, by the Zn^{II} titration experiments,[14] which means that the second Zn^{II} ion is not fully complexed with **1** at low μM concentrations.

$$\mathbf{1} + Zn^{II} \overset{K_1}{\rightleftharpoons} \mathbf{1}\text{–}Zn^{II} \quad (1)$$

$$\mathbf{1}\text{–}Zn^{II} + Zn^{II} \overset{K_2}{\rightleftharpoons} \mathbf{1}\text{–}2Zn^{II} \quad (2)$$

In the fluorescence titration with ATP, the fluorescence emission of **1**–2Zn^{II} underwent a blue shift with a decrease in emission intensity (Figure 4). This response is almost identical to that observed in the formation of the binuclear Zn^{II} complex from the mononuclear upon addition of excess Zn^{II} (Figure 5b). The shape of the UV/Vis spectrum was also changed by ATP to become almost identical to that of the binuclear Zn^{II} complex (Figure 5d). Therefore, it is reasonable that the dual-emission change of the chemosensors upon binding to the nucleoside PPs is due to the dissociation of Zn^{II} from the acridine nitrogen atom as a result of the formation of the ATP-bound complex. The dual-emission sensing mechanism is schematically summarized in Figure 6. In the resting state, the chemosensor predominantly exists as a mononuclear Zn^{II} complex (species I), with coordination between Zn^{II} and the acridine nitrogen atom, in equilibrium with the binuclear Zn^{II} complex (species II). However, the anionic nucleoside PP induces a second Zn^{II} complexation, probably due to its electrostatic and/or coordination assistance, to form the ATP-bound species III, in which the coordination geometry of the first Zn^{II} ion is altered such that the coordination to the acridine nitrogen atom is lost, resulting in the dual-emission change.[15] The similar second Zn^{II} complexation induced by binding with a phosphate anion was also observed in the anthracene-type chemosensor **4**–2Zn^{II}.[10] However, **4**–2Zn^{II} showed a simple fluorescence intensification upon phosphate binding due to the removal of PET quenching by the complexation of Zn^{II} with Dpa. In the case of the acridine-type chemosensors, the second Zn^{II} complexation, induced by the binding of nucleoside PP, results in a change in the coordination geometry of the first

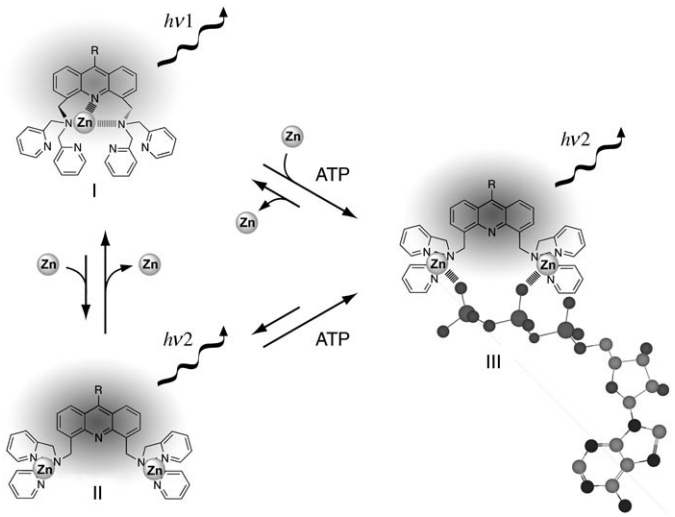

Figure 6. Schematic illustration of the dual-emission sensing mechanism of the acridine chemosensor for nucleopside PPs.[18]

Zn^{II} ion, which perturbs the electronic structure of the acridine fluorophore, leading to the dual-emission change.

Unlike the anthracene-type chemosensor **4**–$2Zn^{II}$, the acridine-type chemosensors did not show fluorescence intensification upon binding to nucleoside PP. This indicates that the acridine-type chemosensor may form a mononuclear Zn^{II} complex with coordination between the Zn^{II} ion and both tertiary amine groups of the two Dpa units (species I in Figure 6), so that the PET-quenching process induced by these amines is fully suppressed even in the mononuclear Zn^{II} complex state. This is supported by the fluorescence Zn^{II} titration plot in Figure 5c, in which the fluorescence intensity is maximized in the presence of 1 equivalent of Zn^{II}. To obtain structural information about the mononuclear Zn^{II} complex of **1**, a ^{1}H NMR spectroscopic study of **1** (1 mM in CD_3OD) was carried out in the presence of $Zn(NO_3)_2$ (1 equiv). However, broad and complicated signals of **1** were observed, which suggests that a number of the Zn^{II} coordination isomers of **1** may exist under such conditions of high concentration. Thus, detailed structural information of the mononuclear Zn^{II} complex (species I) was not obtained at this stage.

Real-time Fluorescence Monitoring of Enzyme Reactions That Involve Nucleoside PP Conversion

With their ability to sense nucleoside PPs selectively (Table 1), these chemosensors can provide a novel ratiometric fluorescence assay for enzymatic metabolism of nucleoside PP. Apyrase, a hydrolytic enzyme that converts ATP or ADP into AMP and inorganic phosphate (P_i),[16] was employed for a proof-of-concept study. It was recently revealed that various types of apyrases play pivotal roles in diverse cellular processes, especially in the control of extracellular signal transduction mediated by nucleoside PPs. Thus, the development of a convenient real-time monitoring system for apyrase activity would be highly desirable for the elucidation of their actions in biological systems.[17] Figure 7a shows the fluorescence difference spectra obtained during apyrase-catalyzed ADP hydrolysis; the blue emission at 428 nm decreased and the green emission at 480 nm increased concurrently. This seesaw-type emission change for **2**–$2Zn^{II}$ is reasonably ascribed to the hydrolysis of ADP into AMP and P_i [Eq. (3)]. The plot of the emission ratio shows that the reaction rate is accelerated with an increase in apyrase concentration (Figure 7b). Kinetic analysis based on first-order reaction kinetics indicates that the rate of ADP hydrolysis is proportional to the amount of apyrase (see Supporting Information).[18] Sequential ATP hydrolysis to AMP [Eq. (4)] could also be monitored by the same fluorescence ratiometry, although detailed kinetic analysis was not done in this case. An issue of concern for this real-time assay is whether **2**–$2Zn^{II}$ decelerates the apyrase-catalyzed reaction by competitive binding to the substrate nucleoside PPs. However, the measured reaction rates in the presence and absence of **2**–$2Zn^{II}$ (0.025 and 0.076 min^{-1}, respectively) with 250 mU of apyrase indicates that significant rate deceleration does not occur.

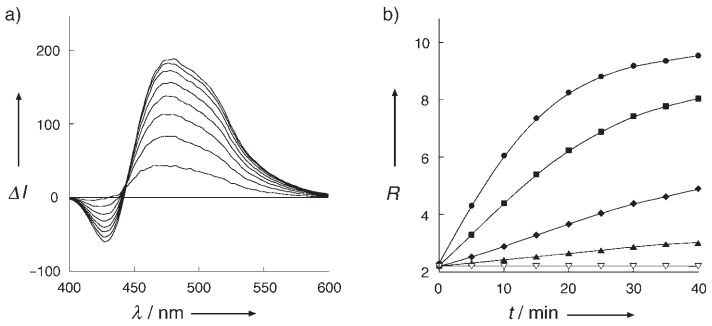

Figure 7. Fluorescence real-time detection of the apyrase-catalyzed hydrolysis of ADP with **2**–$2Zn^{II}$. a) Difference spectra obtained during ADP hydrolysis (0–40 min) against the initial state (0 min) with apyrase (500 mU). b) Time-trace plot of ADP hydrolysis with 1000 (●), 500 (■), 250 (◆), 100 mU (▲), and 0 mU (▽) of apyrase monitored by the emission ratio R ($=I$ at 480/I at 428 nm). Conditions: [**2**–$2Zn^{II}$] = 10 μM, [ADP] = 10 μM, HEPES buffer (50 mM), NaCl (10 mM), pH 7.2, 25 °C, λ_{ex} = 368 nm.

$$ADP \xrightarrow{\text{apyrase}} AMP + P_i \quad (3)$$

$$ATP \xrightarrow{\text{apyrase}} ADP + P_i \xrightarrow{\text{apyrase}} AMP + P_i \quad (4)$$

The chemosensor-based enzyme assay was also applied to the fluorescence monitoring of glycosyltransferase activity.[19] Glycosyltransferases, a superfamily of enzymes in the biosynthesis of oligosaccharides, are vital for all living systems, because they synthesize a variety of oligosaccharides, which play key roles in cell–cell interaction, immune defense, inflammation, and so on.[20] In biological glycosyltransfer processes, nucleotide sugars such as UDP glycosides generally serve as a sugar donor to form a new glycosyl bond with many types of glycosyl acceptors. As nucleotide

sugars are converted into nucleoside PPs during glycosyl transfer, detection of the nucleoside PPs by our chemosensor enables us to monitor this reaction without perturbation of the reactants (Scheme 2). As shown in Table 1, the binding affinity of **2**–2Zn^{II} for UDP is about 10^3 times larger than that for UDP-Gal, which makes it suitable for the quantitative monitoring of glycosyl bond formation by detecting the UDP produced. Thus, we monitored by fluorescence the glycosyl transfer from UDP-Gal to *N*-acetyl glucosamine (GlcNAc) catalyzed by β-1,4-galactosyltranferase (β-1,4-GalT) in the presence of **2**–2Zn^{II} (Scheme 2). As expected, the spectrum of **2**–Zn^{II} changed in a ratiometric manner owing to UDP formation during glycosyl transfer, and the emission ratio increased (Figure 8a). With increasing concentrations of GlcNAc, the increase in the emission ratio was accelerated. The change in the emission ratio was converted into the amount of UDP by a calibration curve, and the data, analyzed with a Lineweaver–Burk plot, gave the Michaelis constant K_M as 1.1 mM (Figure 8b), a value of the same order as that reported (5.1 mM).[21] The chemosensor-based glycosyltransferase assay presented herein is precise and convenient, and does not require any special modification of either glycosyl donor or acceptor. Therefore, this should provide a potentially general method for probing glycosyltransferase activities, which may be superior to conventional methods with radio-labeling or enzyme-reaction-coupling techniques.[22]

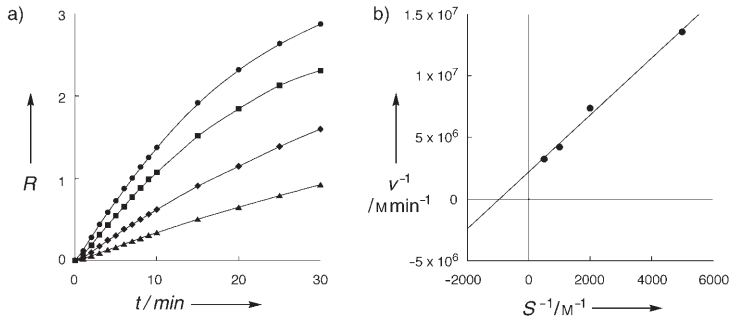

Figure 8. Fluorescence real-time monitoring of the glycosyl-transfer reaction catalyzed by β-1,4-GalT. a) Time-trace plot with **2**–2Zn^{II} in the presence of 2 (●), 1 (■), 0.5 (◆), and 0.2 mM (▲) of GlcNAc monitored by the emission ratio R ($=I$ at 424/I at 486 nm). Assay conditions are described in the Experimental Section. b) Lineweaver–Burk plot of the glycosyl-transfer reaction. v and S refer to the initial rate of the reaction and the concentration of GlcNAc, respectively.

Conclusions

We have developed the dual-emission chemosensors **1**–2Zn^{II} and **2**–2Zn^{II} for nucleoside PP derivatives under neutral aqueous conditions. The chemosensors achieved ratiometric detection of the nucleoside PPs and allowed rapid and precise analysis under complicated biological conditions without the need for special instrumentation or costly enzymes in multistep enzyme-coupled assays, which is an advantage over other ATP-detection systems[3] To our knowledge, this is the first example of a ratiometric fluorescence-sensing system for nucleoside PPs. On the other hand, the detection limit of the chemosensors (10^{-7} M for ATP) may not be low enough to detect the small amounts of nucleoside PPs relevant to various biological events; however, structural optimization of the phosphate binding sites may lead to a sophisticated chemosensor with a stronger binding affinity and higher sensitivity. We also found that the unique shift in emission wavelength induced by nucleoside PP binding is ascribed to the dissociation of the first Zn^{II} ion from the acridine nitrogen atom as a result of the formation of the binu-

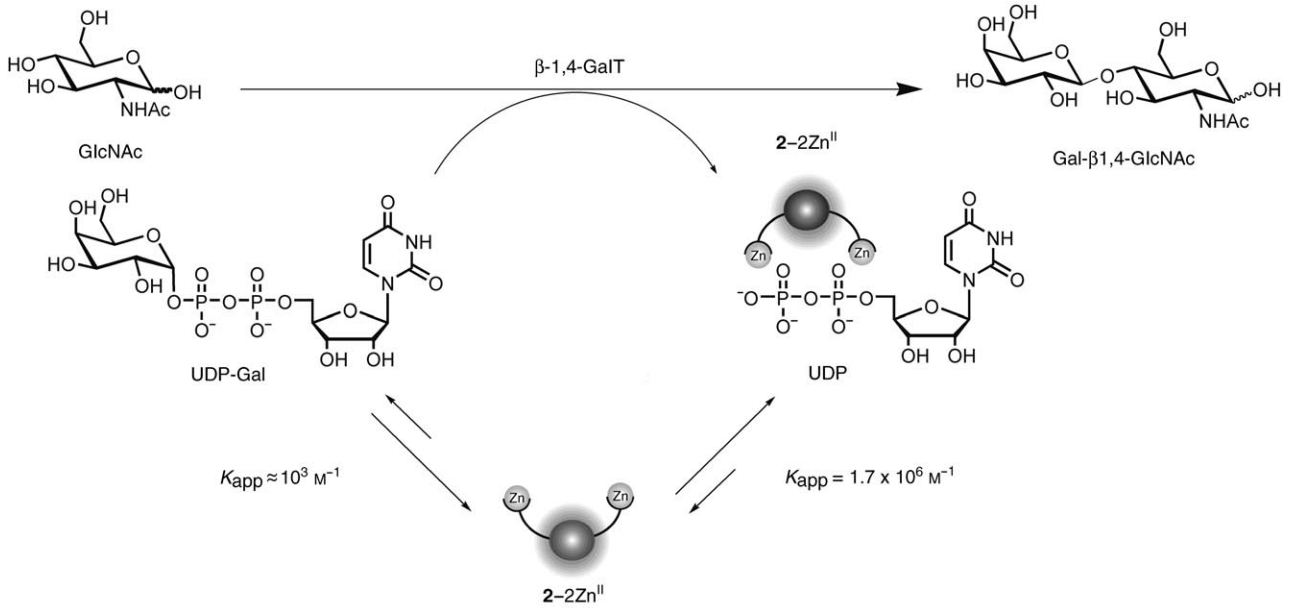

Scheme 2. Fluorescence sensing of the glycosyl-transfer reaction based on the ratiometric detection of UDP by **2**–2Zn^{II}.

clear Zn^{II} complex. The present sensing mechanism based on the anion-induced perturbation of metal–fluorophore interaction may become a general design principle for anion sensing. Furthermore, we have demonstrated that the chemosensor is successful in some biological assays, for example, fluorescence monitoring of apyrase-catalyzed hydrolysis of nucleoside PPs and glycosyl transfer catalyzed by glycosyltransferase. As nucleoside PPs are key intermediates in many biotransformation processes, our methodology should provide a simple and convenient bioanalytical system that is useful for screening small molecular inhibitors and modulators for corresponding enzyme or protein activity. Work on this system is currently underway.

Experimental Section

Synthesis of the Chemosensors

The chemosensors **1**–2Zn^{II}, **2**–2Zn^{II}, and **3**–Zn^{II} were prepared according to the synthetic routes in Scheme 1. Detailed synthetic procedures and compound characterizations are described in the Supporting Information.

Fluorescence Titration with Anions

Fluorescent spectra were recorded on a Perkin–Elmer LS55 spectrometer. The anion titration experiments were conducted with a solution (3 mL) of **1**–2Zn^{II}, **2**–2Zn^{II}, or **3**–Zn^{II} (10 μM) in NaCl (50 mM) and HEPES buffer (50 mM, pH 7.2) at (20±1)°C. The change in fluorescence emission (λ_{ex}=368 nm) was monitored upon the addition of a freshly prepared aqueous stock solution of the anion with a microsyringe. In the case of ATP as the analyte, the titration was carried out with 1 μM of the chemosensor to allow a precise determination of their strong binding. Fluorescence titration curves (λ_{em}=468 nm) were analyzed with nonlinear least-squares curve-fitting analysis with 1:1 binding assumed to evaluate the apparent affinity constant.

Fluorescence Monitoring of Apyrase-Catalyzed Hydrolysis of Nucleoside PPs

Apyrase (isolated from *Solanum tuberosum*, Grade VII, activity ratio ATPase/ADPase≈1:1) was purchased from Sigma–Aldrich. A solution of **2**–2Zn^{II} (10 μM) and the nucleoside PP (ATP or ADP; 10 μM) in assay buffer (3 mL, 50 mM HEPES, 10 mM NaCl, pH 7.2) was preincubated (25°C) in a quartz cell. An appropriate amount (100–1000 mU) of apyrase was added to the solution, and the quartz cell was immediately placed in the fluorescence spectrometer. The emission spectrum (λ_{em}= 400–600 nm, λ_{ex}=368 nm) was recorded automatically at each reaction time point (scan time=5 s) at 25°C. The rate of change of the fluorescence-emission ratio R was converted into the rate of ADP degradation by using a calibration curve obtained from fluorescence titration under assay conditions. The ADP degradation curve obtained was analyzed by curve-fitting analysis based on first-order reaction kinetics to obtain the apparent reaction rate.

Fluorescence Monitoring of Glycosyl Transfer Catalyzed by β-1,4-GalT

β-1,4-GalT (human, EC 2.4.1.22) was purchased from Toyobo (Japan). A solution of β-1,4-GalT (16 mU), GlcNAc (0.2, 0.5, 1, 2 mM), **2**–2Zn^{II} (4 mM), and $Zn(NO_3)_2$ (24 μM) in assay buffer (500 μL, 50 mM HEPES, 50 mM NaCl, 0.1 mM $MgCl_2$, pH 7.2) was preincubated in a quartz cell at 25°C. $Zn(NO_3)_2$ was added to suppress the inhibition effect of β-mercaptoethanol in a solution of β-1,4-GalT. After addition of UDP-Gal (final concentration=20 μM), the emission spectrum (λ_{em}=400–600 nm, λ_{ex}= 368 nm) was recorded automatically at each reaction time point (scan time=5 s) at 25°C. The rate of change of R was converted into initial velocity V_i by using a calibration curve obtained from fluorescence titration under assay conditions. The data were analyzed with a Lineweaver–Burk plot to obtain the Michaelis constant K_M.

[1] B. Alberts, A. Johnson, J. Lewis, M. Raff, K. Roberts, P. Walter, *Molecular Biology of the Cell*, *4th ed.*, Newton, Tokyo, **2002**.

[2] a) G. Burnstock, *Pharmacol. Rev.* **2006**, *58*, 58–86; b) A. V. Gourine, E. Llaudet, N. Dale, M. Spyer, *Nature* **2005**, *436*, 108–111.

[3] a) *A Guide to Fluorescent Probes and Labeling Technologies*, *10th ed.* (Ed.: M. T. Z. Spence), Invitrogen, Eugene, **2005**, chap. 10; b) E. Llaudet, S. Hatz, M. Droniou, N. Dale, *Anal. Chem.* **2005**, *77*, 3267–3273; c) S. Ikeno, T. Haruyama, *Sens. Actuators B* **2005**, *108*, 608–612; d) R. C. H. Kwan, H. F. Leung, P. Y. T. Hon, H. C. F. Cheung, K. Hirota, R. Renneberg, *Anal. Biochem.* **2005**, *343*, 263–267; e) J. Wang, Y. Jiang, C. Zhou, X. Fang, *Anal. Chem.* **2005**, *77*, 3542–3546; f) S. Hayashi, A. Hazama, A. K. Dutta, R. Z. Sabirov, Y. Okada, *Sci. STKE* **2004**, *258*, 14–25; g) S. W. Schneider, M. E. Egan, B. P. Jena, W. B. Guggino, H. Oberleithner, J. P. Geibel, *Proc. Natl. Acad. Sci. USA* **1999**, *96*, 12180–12185; h) R. Reza, E. Kobatake, M. Aizawa, G. R. Dubyak, *Am. J. Physiol.* **1999**, *276*, C267–C278; i) F. Schubert, *Sens. Actuators B* **1993**, *11*, 531–535; j) Y. Adachi, M. Sugawara, K. Taniguchi, Y. Umezawa, *Anal. Chim. Acta* **1993**, *281*, 577–584.

[4] a) R. Martínez-Máñez, F. Sancenón, *Chem. Rev.* **2003**, *103*, 4419–4476; b) P. D. Beer, P. A. Gale, *Angew. Chem.* **2001**, *113*, 502–532; *Angew. Chem. Int. Ed.* **2001**, *40*, 486–516.

[5] a) S. Aoki, E. Kimura, *Rev. Mol. Biotechnol.* **2002**, *90*, 129–155; b) J. Y. Kwon, N. J. Singh, H. N. Kim, S. K. Kim, K. S. Kim, J. Yoon, *J. Am. Chem. Soc.* **2004**, *126*, 8892–8893; c) H. Abe, Y. Mawatari, H. Teraoka, K. Fijimoto, M. Inouya, *J. Org. Chem.* **2004**, *69*, 495–504; d) D. H. Lee, S. Y. Kim, J.-I. Hong, *Angew. Chem.* **2004**, *116*, 4881–4884; *Angew. Chem. Int. Ed.* **2004**, *43*, 4777–4780; e) L. Fabbrizzi, N. Marcotte, F. Stomeo, A. Taglietti, *Angew. Chem.* **2002**, *114*, 3965–3968; *Angew. Chem. Int. Ed.* **2002**, *41*, 3811–3814; f) F. Sancenón, A. B. Descalzo, R. Martînez-Máñez, M. A. Miranda, J. Soto, *Angew. Chem.* **2001**, *113*, 2710–2713; *Angew. Chem. Int. Ed.* **2001**, *40*, 2640–2643; g) S. E. Schneider, S. N. O'Neil, E. V. Anslyn, *J. Am. Chem. Soc.* **2000**, *122*, 542–543; h) J. I. Bruce, R. S. Dickins, L. J. Govenlock. T. Gunnlaugsson, S. Lopinski, M. P. Lowe, D. Parker, R. D. Peacock, J. J. B. Perry, S. Aime, M. Botta, *J. Am. Chem. Soc.* **2000**, *122*, 9674–9684; i) H. Fenniri, M. W. Hosseini, J.-M. Lehn, *Helv. Chim. Acta* **1997**, *80*, 786–803; j) M. W. Hosseini, A. J. Blacker, J.-M. Lehn, *J. Am. Chem. Soc.* **1990**, *112*, 3896–3904.

[6] Bioanalytical application of a phosphate-anion sensor: a) M. S. Han, D. H. Kim, *Bioorg. Med. Chem. Lett.* **2003**, *13*, 1079–1082; b) S. Mizukami, T. Nagano, Y. Urano, A. Odani, K. Kikuchi, *J. Am. Chem. Soc.* **2002**, *124*, 3920–3925; c) D. H. Vance, A. W. Czarnik, *J. Am. Chem. Soc.* **1994**, *116*, 9397–9398.

[7] a) *The Handbook—A Guide to Fluorescent Probes and Labeling Technologies*, *10th ed.* (Ed.: R. P. Haigland), Invitrogen, Eugene, **2005**, chap. 19; b) B. Valeur, I. Leray, *Coord. Chem. Rev.* **2000**, *205*, 3–40; c) M. Taki, J. L. Wolford, T. V. O'Halloran, *J. Am. Chem. Soc.* **2003**, *126*, 712–713; d) M. M. Henary, Y. Wu, C. J. Fahrni, *Chem. Eur. J.* **2004**, *10*, 3015–3025; e) Y. Suzuki, H. Komatsu, T. Ikeda, N. Saito, S. Araki, D. Citterio, H. Hisamoto, Y. Kitamura, T. Kubota, J. Nakagawa, K. Oka, K. Suzuki, *Anal. Chem.* **2002**, *74*, 1423–1428; f) G. Grynkiewicz, M. Poenie, R. Y. Tsien, *J. Biol. Chem.* **1985**, *260*, 3440–3450.

[8] a) A. Ojida, H. Nonaka, Y. Miyahara, S. Tamaru, K. Sada, I. Hamachi, *Angew. Chem.* **2006**, *118*, 5518–5521; *Angew. Chem. Int. Ed.* **2006**, *45*, 5644–5647; b) Y. Bretonniére, M. J. Cann, D. Parker, R. Slater, *Chem. Commun.* **2002**, 1930–1931; c) J.-H. Liao, C.-T. Chen, J.-M. Fang, *Org. Lett.* **2002**, *4*, 561–564; d) K. Choi, A. D. Hamilton, *Angew. Chem.* **2001**, *113*, 4030–4033; *Angew. Chem. Int. Ed.* **2001**, *40*, 3912–3915.

[9] a) A. Gafni, L. Brand, *Chem. Phys. Lett.* **1978**, *58*, 346–350; b) R. Snyder, A. C. Testa, *J. Lumin.* **1990**, *47*, 35–39.

[10] a) A. Ojida, I. Hamachi, *Bull. Chem. Soc. Jpn.* **2006**, *79*, 35–46; b) A. Ojida, Y. Mito-oka, K. Sada, I. Hamachi, *J. Am. Chem. Soc.* **2004**, *126*, 2454–2463; c) A. Ojida, T. Kohira, I. Hamachi, *Chem. Lett.* **2004**, 1024–1025; d) A. Ojida, Y. Mito-oka, M. Inoue, I. Hamachi, *J. Am. Chem. Soc.* **2002**, *124*, 6256–6258.

[11] M. S. Newman, W. H. Powell, *J. Org. Chem.* **1961**, *26*, 812–815.

[12] X-ray diffraction data were collected at 120 K on a Rigaku RAPID-HR diffractometer with a 2D area detector with graphite-monochromated $Mo_{K\alpha}$ radiation ($\lambda = 0.7107$ Å). Crystal data for **1**–$2Zn^{II}{\cdot}4NO_3{\cdot}MeOH$: $C_{40}H_{38}ClN_{11}O_{13}Zn_2$, $M_r = 1047.02$, triclinic, space group $P\bar{1}$, $a = 8.536(2)$, $b = 14.200(3)$, $c = 19.080(5)$ Å, $V = 2134.8(8)$ Å^3, $a = 67.860(9)$, $b = 88.224(9)$, $c = 85.251(6)°$, $Z = 2$, $\rho_{calcd} = 1.629$ g cm^{-3}, $\mu = 1.267$ mm^{-1}, crystal size $0.10 \times 0.20 \times 0.50$ mm^3, 34667 collected reflections, 22056 unique. $R1 = 0.062$ for 9619 reflections with $I > 2\sigma(I)$, $wR2 = 0.1970$ ($I > 3\sigma(I)$), GOF = 1.390. All calculations were performed with the CrystalStructure software package (Rigaku). Direct methods (SIR92) were used for the structure solution. The structure was refined by full-matrix least-squares using observed reflections based on F^2. All non-hydrogen atoms were refined with anisotropic displacement parameters, and hydrogen atoms were placed in idealized positions with isotropic displacement parameters relative to the connected non-hydrogen atoms and refined in riding geometries. CCDC-605914 contains the supplementary crystallographic data for this paper. These data can be obtained free of charge from The Cambridge Crystallographic Data Centre at www.ccdc.cam.ac.uk/data_request/cif.

[13] Compound **6a** also showed a bathochromic emission shift by protonation of the acridine nitrogen atom, that is, the emission maximum at 439 nm under neutral or alkaline conditions underwent a red shift to 510 nm under acidic conditions (see Supporting Information).

[14] The fluorescence Zn^{II} titration of **1** (1 μM in HEPES (10 mM, pH 7.2)/MeOH = 1:1) showed that the fluorescence intensity increased linearly with the addition of up to 1 equivalent of Zn^{II}, indicating that the complexation constant of the first Zn^{II} ion (K_1) is over 10^7 M^{-1}, although K_1 in aqueous solution (10 mM HEPES, pH 7.2) could not be accurately evaluated owing to the low solubility of the Zn^{II}-free ligand **1**. The complexation constant of the second Zn^{II} ion (K_2) was evaluated by the fluorescence and UV/Vis Zn^{II} titration of **1** (20 μM) in aqueous HEPES buffer (10 mM, pH 7.2).

[15] Fluorescence titration of **1**–$2Zn^{II}$ with AMP (10 mM HEPES, pH 7.2) showed that the binding became stronger on addition of excess Zn^{II} ions. For example, in the presence of 60 and 100 μM of extra free $Zn(NO_3)_2$, the binding affinity reached 6.1×10 and 1.2×10^6 M^{-1}, respectively, which is about six and 12 times larger, respectively, than the original value for **1**–$2Zn^{II}$ ($K_{app} = 1.1 \times 10^5$ M^{-1}). This result clearly indicates that the actual species for nucleoside PP binding is the binuclear Zn^{II} complex (species II in Figure 6) and supports the proposed sensing mechanism, which involves the second Zn^{II} complexation from the mononuclear species I.

[16] a) H. Zimmermann, *Trends Pharmacol. Sci.* **1999**, *20*, 231–236; b) A. M. Kettlun, L. Uribe, V. Calvo, S. Silva, J. Rivera, M. Mancilla, M. A. Valenzuela, A. Traverso-Cori, *Phytochemistry* **1982**, *21*, 551–558.

[17] S. Karamohamed, G. Guidotti, *Biotechniques* **2001**, *31*, 420–425.

[18] As the K_M value of apyrase for ADP ($K_M = 100$–250 μM) is much larger than the ADP concentration (10 μM) used in the assay, the rate of ADP hydrolysis based on first-order reaction kinetics was employed in the quantitative reaction analysis.

[19] J. Wongkongkatep, Y. Miyahara, A. Ojida, I. Hamachi, *Angew. Chem.* **2006**, *118*. 681–684; *Angew. Chem. Int. Ed.* **2006**, *45*, 665–668.

[20] a) A. Holemann, P. H. Seeberger, *Curr. Opin. Biotechnol.* **2004**, *15*, 615–622; b) C. R. Bertozzi, L. L. Kiessling, *Science* **2001**, *291*, 2357–2364.

[21] J.-P. Prieels, M. Dolmans, *Eur. J. Biochem.* **1976**, *66*, 579–582.

[22] a) M. M. Palcic, K. Sujino, *Trends Glycosci. Glycotechnol.* **2001**, *13*, 361–370; B. Ramakrishnan, E. Boeggeman, P. K. Qasba, *Biochemistry* **2004**, *43*, 12513–12522; b) K. Washiya, T. Furuike, F. Nakajima, Y. C. Lee, S.-I. Nishimura, *Anal. Biochem.* **2000**, *283*, 39–48; c) H. C. Hang, C. Yu, M. R. Pratt, C. R. Bertozzi, *J. Am. Chem. Soc.* **2003**, *126*, 6–7; d) H. Liu, T. K. Ritter, R. Sadamoto, P. S. Sears, M. Wu, C. H. Wong, *ChemBioChem* **2003**, *4*, 603–609.

Received: May 2, 2006

